

Characterization of interfacial reactions in magnetite tunnel junctions with transmission electron microscopy

Yingguo Peng,^{a)} Chando Park, Jian-Gang Zhu, Robert M. White, and David E. Laughlin
Data Storage Systems Center, Carnegie Mellon University, Pittsburgh, Pennsylvania 15213

(Presented on 7 January 2003)

To make a uniform AlO_x barrier layer in tunnel junctions, a thin layer of Al is often sputtered first and then oxidized. In this study, we sputtered a thick layer of Al onto Fe_3O_4 and then employed high resolution transmission electron microscopy and x-ray energy dispersive spectroscopy to investigate the interfacial microstructures. Two new layers have been found and investigated at the $\text{Al}/\text{Fe}_3\text{O}_4$ interface. The interfacial reaction has been determined to be: $\text{Fe}_3\text{O}_4 + \text{Al} \Rightarrow \text{Fe} + (a)\text{AlO}_x$, where a denotes the amorphous state. The consequence of the interfacial reaction to transport properties is also discussed. © 2004 American Institute of Physics. [DOI: 10.1063/1.1688535]

I. INTRODUCTION

Half metallic magnetite (Fe_3O_4) has been thought to be one of the most promising materials for magnetic tunnel junction (MTJ) electrodes to achieve extremely high magnetoresistance ratio.¹ However, experiments on Fe_3O_4 systems have not produced the expected results.^{2,3} It is well known that the interfacial microstructure is critical to the transport properties of tunnel junctions. In our pursuit of large magnetoresistance with Fe_3O_4 based tunnel junctions, we have found that the interfacial state dramatically changes the magnetoresistance ratio.⁴ A uniform AlO_x barrier layer is usually fabricated by a process in which a thin layer of Al is first sputtered and then oxidized naturally or with plasma enhancement. However, the interface and barrier layer of the Fe_3O_4 tunnel junctions are not yet fully understood. Since high resolution transmission electron microscopy (HRTEM) has the ability to resolve the atomic arrangement in a nano-size area, it has been employed to investigate interfacial local microstructures.⁵ In this study, a thick layer of Al was deposited onto Fe_3O_4 , and the interfacial microstructure has been characterized. The affect of the interfacial microstructure on the junction properties is also discussed.

II. EXPERIMENT

Thin films were deposited onto Si or oxidized Si wafers by either rf diode or dc magnetron sputtering. An Fe_3O_4 layer was deposited by the reactive sputtering of Fe with flowing oxygen and argon. The AlO_x barrier layer in the MTJ structures was produced by the plasma oxidation of a thin layer of Al. The details of the thin film fabrication have been described previously.⁴ The preparation of transmission electron microscope (TEM) samples follows the procedures described in Ref. 5. The Al foil sandwiched by two slices of thin film samples yields reproducibly high quality cross-sectional TEM specimens. Bright field micrographs and selected area electron diffraction (SAED) patterns were taken

on a JEOL JEM-2010 electron microscope. High resolution observations and chemical compositional investigations were accomplished on an FEI Tecnai F20 microscope equipped with an energy filtering TEM system and x-ray energy dispersive spectroscopy (EDS). The analysis of HRTEM images was carried out with DigitalMicrograph from Gatan Inc.

III. RESULTS AND DISCUSSION

Figure 1 represents the microstructure of a single layer of an Fe_3O_4 thin film deposited by reactive sputtering. The sample was annealed at 380°C for 30 min. When compared to the Fe_3O_4 thin films sputtered from oxide targets,⁶ it is noted that reactive sputtering gives rise to a smaller grain size, fewer crystallographic defects, and a smoother surface.⁴ The diffraction rings of the SAED pattern in Fig. 1(a) fit very well with the Fe_3O_4 phase, as shown in Fig. 1(b). The x-ray profile was calculated with CaRIne Crystallography

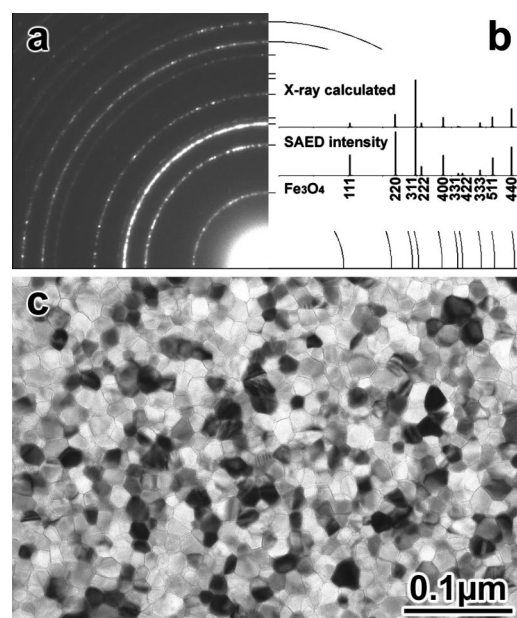


FIG. 1. SAED pattern and micrograph of 100 nm Fe_3O_4 thin film annealed at 380°C for 30 min.

^{a)}Author to whom correspondence should be addressed; electronic mail: yingguo@ece.cmu.edu

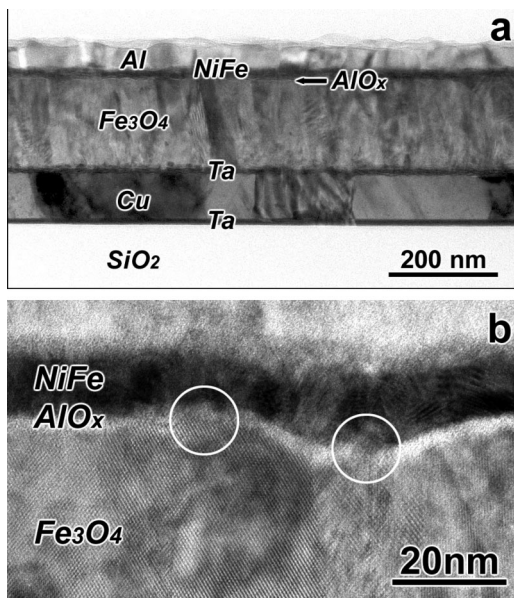


FIG. 2. Cross-section images of MTJ of oxidized-Si/Ta₅nm/Cu₁₀₀nm/Ta_{2.5}nm/Fe₃O₄₂₀₀nm/AlO_x₂nm/NiFe₁₀nm/Al₅₀nm.

(©1989–1998 C. Boudias & D. Monceau) and converted to a plot of peak intensity versus $1/d$ spacing. The SAED intensity profile was obtained by integrating the reflection intensities along the radius direction. All the reflections are present and have been indexed under the peaks in Fig. 1(b). The intensities of the SAED pattern follow closely the calculated values taking into account the dynamic effect of electron diffraction. The good match of peak positions between these two profiles indicates that the thin film is composed of only grains of the Fe₃O₄ crystal phase. The existence of all the reflections with intensities close to the x-ray profile also implies that the Fe₃O₄ grains are randomly oriented. The plan-view image in Fig. 1(c) shows well-defined grains with the grain size on the order of 20 nm. A noticeable feature in the image is the grain boundary network. The grain boundaries have a uniform width and a consistent gray contrast, which can be attributed to an amorphous phase at the grain boundaries. Although voids at boundaries could also produce a uniform contrast, they should be the brightest due to the zero scattering of electrons. However, in the image of Fig. 1(c), many grains are brighter than the boundaries due to their off-zone-axis orientations. We conclude the boundary phase is amorphous. The gray contrast of amorphous material comes from its background scattering.

We fabricated MTJs where Fe₃O₄ is used as the bottom electrode and AlO_x is used as the barrier. The MTJ stacking sequence was Ta₅nm/Cu₁₀₀nm/Ta_{2.5}nm/Fe₃O₄₂₀₀nm/AlO_x₂nm/NiFe₁₀nm/Al₅₀nm, as shown in Fig. 2(a). However, the magnetoresistance (MR) curves were found to be very noisy and the MR ratio is low (~2.5%) A high magnification cross-sectional image of the junction shown in Fig. 2(b) reveals a wavy interface and many pinholes as indicated by circles in the image. Something has occurred during the barrier layer deposition. The AlO_x barrier layer was fabricated by a plasma oxidation process, in which a thin layer of Al was first deposited and then oxidized

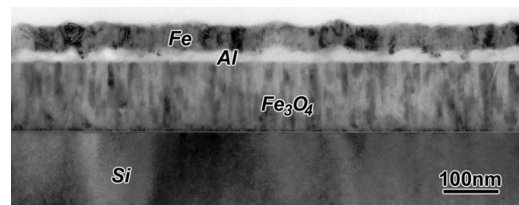


FIG. 3. Cross-sectional image of Si/Fe₃O₄₁₂₅nm/Al₂₅nm/Fe₄₀nm.

with an oxygen plasma. This process is widely used to achieve a uniform and high quality Al oxide barrier in MTJs.

In order to study the irregularity at the barrier layer, we deposited a thicker Al layer between Fe₃O₄ and Fe without the plasma oxidation process. Figure 3 shows the cross section of the structure Si/Fe₃O₄₁₂₅nm/Al₂₅nm/Fe₄₀nm. The fine microstructure of the Fe₃O₄/Al interface was investigated with HRTEM. Figure 4 reproduces a typical Al/Fe₃O₄ interface. The bottom part (region A) can be easily identified as [011] Al, and the top part (region B) shows lattice planes of the Fe₃O₄ phase. Two extra layers are found to form between the Al and the Fe₃O₄: an amorphous layer adjacent to Al and an unidentified crystalline phase (region C) on the Fe₃O₄ side. It is also noticeable that the amorphous layer is bridged by small crystalline grains at some places and the unidentified crystalline phase overlapping with the Fe₃O₄.

In order to identify the phase in region C, lattice spacings must be measured accurately. The Fourier transformation converts a two dimensional (2D) HRTEM image into a pattern similar to a SAED (diffractogram). The spacings between a pair of spots in the diffractogram correspond to an average of the plane spacings in HRTEM image and can be measured digitally to a high degree of accuracy. This technique has demonstrated the capability of characterizing lattice deformation in a very thin layer.^{5,7} Figure 5 shows the Fourier transforms from regions A, B, and C in Fig. 4, and the corresponding line scan profiles across spot pairs, respectively. The line profiles exhibit distinct sharp peaks so that distance between peaks can be easily determined. The mea-

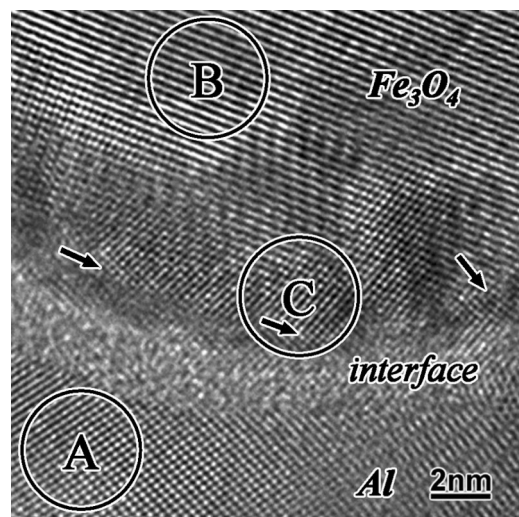


FIG. 4. HRTEM image of Al/Fe₃O₄ interface.

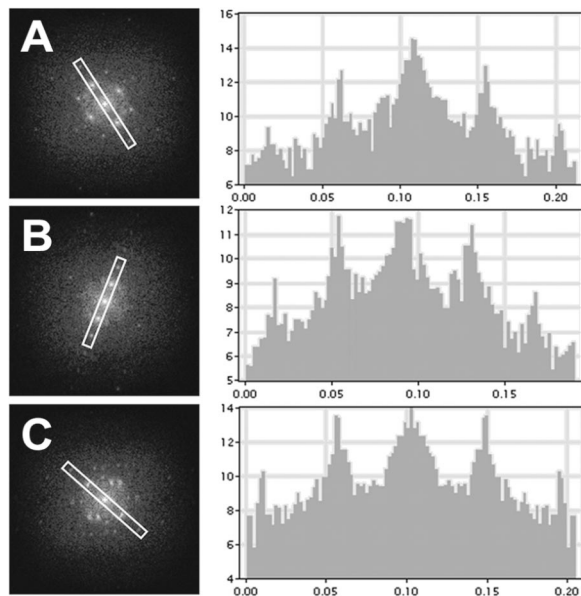


FIG. 5. Fourier transforms and the line profiles from the regions A, B, and C of Fig. 4.

sured spacings $2R$, corresponding d values, and the fitting result are summarized in Table I. The data are normalized with Al (200) as a reference. It is confirmed that B fits very well with Fe_3O_4 (311). The lattice spacing in region C is determined to be 2.04 \AA , with an error range estimated as about $\pm 1\%$. Besides, as indicated by the arrows in Fig. 4, the lattice planes form squares at the very edge of the Fe_3O_4 side, where there is no overlapping with the Fe_3O_4 . Among the phases consisting of Fe/Al/O that exist at ambient temperature and pressure, we found that Fe, Fe_3Al , FeAl, and Al could all form this square lattice image. These phases have either a body-centered cubic (bcc) lattice ($A2$ or $B2$) with a close to $2.04 \text{ \AA} \times \sqrt{2}$ (2.88 \AA) or face-centered cubic lattice with a close to $2.04 \text{ \AA} \times 2$ (4.08 \AA). Thus, the phase in region C cannot be determined by simply matching d spacings among the four candidates. However, since the amorphous AlO_x layer, which will be discussed below, forms around Al grains and protects the Al element from diffusing through the region C phase, which is on the other side of the AlO_x layer, should not contain any Al. Therefore, Al, FeAl, and Fe_3Al are ruled out, and the phase in region C is bcc Fe.

EDS were collected from each of the regions A, B, C and the amorphous layer. As is characteristic of EDS, the effect from adjacent areas is inevitable. The overlapping of phases that can be seen in Fig. 4 prevented us from obtaining EDS spectra that can be unambiguously attributed to a single phase. Nevertheless, region A has only one significant peak of Al, and B has both Fe and O peaks, which represent the Al and Fe_3O_4 very well, respectively. The fact that Fe is the strongest peak in region C is consistent with our above interpretation. In the spectrum collected from the amorphous

TABLE I. Identification of the lattice planes in the HRTEM image.

	Region		
	A	B	C
$2R$ ($1/\text{\AA}$)	0.494	0.392	0.489
Measured d_m (\AA)	2.024	2.55	2.04
Fitted d_f (\AA)	Reference Al (200)	2.532 Fe_3O_4 (311)	2.027 Fe (110)

region, the Al peak is the strongest and O is also fairly strong. Based on the amorphous state and the EDS peak intensities, it is reasonable to consider that the amorphous region corresponds to aluminum oxide, AlO_x . Therefore, the interface reaction can be written as: $\text{Fe}_3\text{O}_4 + \text{Al} \Rightarrow \text{Fe} + (a)\text{AlO}_x$, where a stands for the amorphous state. It is known that the heats of formation of Al_2O_3 and Fe_3O_4 are -266.6 and -130.4 kcal/mole, respectively.⁸ Thus Al is more reactive with oxygen than is Fe, and hence the reaction as written is thermodynamically favorable.

It is well known that oxidation and reduction occur at many metal–oxide interfaces and induce interfacial heterogeneity.⁹ In the design of MTJs, reactions must be taken into account when metal–oxide interfaces are involved. In Ref. 4, we reported the appearance of extra phases when Fe_3O_4 is used as the top electrode. In this article we reported the reaction problem at the interface when magnetite is used as the bottom electrode. Thus, a new strategy is required to fabricate tunnel junctions involving Fe_3O_4 .

IV. SUMMARY

We have characterized the interfacial reaction by HRTEM in the Fe_3O_4 MTJs and the reaction products have been deduced. The reaction occurs in the fabrication process of AlO_x barrier layer, which involves the deposition of metallic Al layer onto the Fe_3O_4 electrode, and causes the poor transport properties of the junctions.

ACKNOWLEDGMENT

The authors gratefully acknowledge the Data Storage Systems Center for its financial support of the research project.

¹Z. Zhang and S. Satpathy, Phys. Rev. B **44**, 13319 (1991).

²X. W. Li, A. Gupta, G. Xiao, W. Qian, and V. P. Dravid, Appl. Phys. Lett. **73**, 3282 (1998).

³K. Aoshima and S. X. Wang, J. Appl. Phys. **93**, 7954 (2003).

⁴C. Park, Y. Shi, Y. Peng, K. Barmark, J. G. Zhu, and D. E. Laughlin, IEEE Trans. Magn. **39**, 2806 (2003).

⁵Y. Peng, T. Ohkubo, and D. E. Laughlin, Scr. Mater. **48**, 937 (2003).

⁶Y. Peng, C. Park, and D. E. Laughlin, J. Appl. Phys. **93**, 7957 (2003).

⁷Y. Peng, J. G. Zhu, and D. E. Laughlin, J. Appl. Phys. **91**, 7676 (2002).

⁸T. B. Reed, *Free Energy of Formation of Binary Compounds: An Atlas of Charts for High-Temperature Chemical Calculations* (MIT Press, Cambridge, MA, 1971).

⁹R. Cheng, C. N. Borca, N. Pilet, B. Xu, L. Yuan, B. Doudin, and S. H. Liou, Appl. Phys. Lett. **81**, 2109 (2002).